2014

Evolution of Land Surface Air Temperature Trend

Fei Ji, Zhaohua Wu, Jianping Huang, and E. Chassignet

Evolution of land surface air temperature trend

Fei Ji[1,2,4], Zhaohua Wu[3,4], Jianping Huang[1,2], and Eric P. Chassignet[3,4]

1. College of Atmospheric Sciences
Lanzhou University, Lanzhou, China

2. Key Laboratory for Semi-Arid Climate Change of the Ministry of Education
College of Atmospheric Sciences
Lanzhou University, Lanzhou, China

3. Department of Earth, Ocean and Atmospheric Science
Florida State University
Tallahassee, Florida, USA

4. Center for Ocean-Atmospheric Prediction Studies
Florida State University
Tallahassee, Florida, USA

Submitted to *Nature Climate Change*
March 2014

Corresponding author: Dr. Zhaohua Wu
Department of Earth, Ocean and Atmospheric Science
Center for Ocean-Atmospheric Prediction Studies
Florida State University
Tallahassee, Florida
zwu@fsu.edu

The global climate has been experiencing significant warming at an unprecedented pace in the past century[1, 2]. This warming is spatially and temporally non-uniform, and one needs to understand its evolution in order to better evaluate its potential societal and economic impact. In this paper, the evolution of global land surface temperature trend in the last century is diagnosed using the spatial–temporally multidimensional ensemble empirical mode decomposition method[3]. We find that the noticeable warming (>0.5 K) started sporadically over the global land and accelerated until around 1980. Both the warming rate and spatial structure have changed little since. The fastest warming in recent decades (>0.4 K/decade) occurred in northern midlatitudes. From a zonal average perspective, noticeable warming (>0.2 K since 1900) first took place in the subtropical and subpolar regions of the Northern Hemisphere, followed by subtropical warming in the Southern Hemisphere. The two bands of warming in the Northern Hemisphere expanded from 1950 to 1985 and merged to cover the entire Northern Hemisphere.

In the past two decades, a large body of studies have examined surface air temperature (SAT) change and variability over the last 160 years on global and regional scales and the resulting social and economic impacts[1, 2, 4, 5]. However, many of these studies focused on averaged warming over that time-span using traditional statistical methods, such as straight line fitting, which can only extract warming at a constant rate. Since warming on different spatial scales is not uniform over time, such time-unvarying change may not effectively reveal the true nature of climate variability and change. To address this problem, a diagnosis of the evolution of warming on different spatial–temporal scales is necessary.

In this study, we focus on how the land surface air temperature trend has evolved since 1900. Traditionally, the shape of a trend is determined *a priori*, e.g., a time-unvarying linear trend or a time-varying exponential trend. Often, little justification is given for why a particular shape of functional form should be used, and the traditional trend lacks the capability of reflecting the hidden nonlinear and nonstationary nature of a time series. Here we adopt a logically consistent definition of trend provided by *Wu et al.*[6], i.e., a trend of a time series is "*an intrinsically fitted monotonic function or a function in which there can be at most one extremum within a given data span*." This definition requires that any identifiable oscillatory components contained in this time-span be removed. Also, an intrinsic trend should require no *a priori* functional form and can vary with time.

The method we use to separate spatial-temporally varying trend and spatially non-uniform variability of different timescales is the multidimensional ensemble empirical mode decomposition (MEEMD)[3], a method based on ensemble empirical mode decomposition (EEMD)[7-9] for time series analysis. In EEMD, a time series at a grid point *x(t)* is decomposed using EEMD in terms of adaptively obtained, amplitude-frequency modulated oscillatory components C_j (j =1, 2, …, n) and a residual R_n, a curve either monotonic or containing only one extremum from which no additional oscillatory components can be extracted:

$$x(t) = \sum_{j=1}^{n} C_j(t) + R_n(t). \qquad (1)$$

Examples of such decomposition can be found in Figs. 2 and 4 of the accompanied Supplementary Information (SI). As demonstrated in SI and previous studies[6, 16], the extracted trend (R_n) follows no *a priori* shape and varies with time after the intrinsic variability of multidecadal and shorter timescales is removed. This trend also has low sensitivity to the extension (addition) of new data. The latter property guarantees that the physical interpretation within specified time intervals does not change with the addition of new data, consistent with a physical constraint that the subsequent evolution of a physical system cannot alter the reality that has already happened.

For multidimensional spatial-temporal data, we piece together similar timescale components of data series from all grids to form a temporal evolution of the spatially coherent structure of that timescale. This is the essence of MEEMD, with more details introduced in SI and *Wu et al.*[3]. Clearly, MEEMD is a temporally and spatially local method, in contrast to popular domain-dependent methods (e.g., empirical orthogonal function analysis), for analyzing spatial-temporal climate data. It is anticipated that the temporal and spatial locality provides a better chance for the trend to identify the underlying physical information of data (see SI for more discussion). Both EEMD and MEEMD have been widely applied in climate research[10-20].

The data used in this study are the monthly land surface air temperature from the Climatic Research Unit, University of East Anglia, for the period January 1901 to December 2009, with a horizontal resolution of 0.5º × 0.5º [21]. Since we are interested in centennial-scale global land warming, the data span adopted for the trend in this study is from 1901 to 2009, with the variability of multidecadal and shorter timescales removed.

Due to the time-varying nature of the trend defined above, the averaged warming rate (slope) of trend over a given time interval cannot reflect well how the trend has evolved. To overcome this deficiency, here we diagnose the value increment of the EEMD trend at a given time from the reference time of 1901, i.e., $Trend_{EEMD}(t) = R_n(t) - R_n(1901)$, representing accumulated warming from 1901. This definition also facilitates the comparison of EEMD trend with the corresponding linear trend. The spatial evolution of the accumulated warming by a given time is displayed in Fig. 1. Before 1950, noticeable accumulated warming (>0.5K) or cooling (<-0.5K) appeared to be sporadically distributed in space, mainly along subtropical bands around 30°S and 30°N and in the subpolar region around 60°N. (The statistical significance against various null hypotheses is presented in SI.) The subtropical bands coincide with the downward branches of Hadley cells. The other noticeable warming region appeared in western Africa near the southern edge of the Sahara Desert. All these regions are arid or semiarid. The earlier sporadic warming has been expanding since 1950. By 1990, the warming regions had expanded across almost all the northern midlatitudes. The warmest regions in the Northern Hemisphere do not correspond to the original two bands near 30°N or 60°N; rather, they are in between, i.e., located in midlatitude semiarid regions. The amplitude and spatial patterns of the statistically significant EEMD trend from 1901 to 2009 are slightly different from those of the linear trend over the same period. However, the evolution of the warming pattern cannot be revealed by the linear trend (Fig. 1*h*).

Since the trends obtained are time-varying, their corresponding warming/cooling rates, which can be determined by calculating temporal derivatives of trends, are also temporally and spatially local quantities. The warming and cooling rates are displayed in Fig. 2. Before 1950, there were both moderate warming and weak cooling regions. The cooling regions shrank, and most of them turned into warming regions with an accelerated pace of warming in the next three decades. By 1980, except for the weak cooling in the northern tip of Greenland and in the vicinity of the Andes, almost all the global land had been warming. The warming rates over the global land have changed little since. The strongest warming occurred in the northern mid-latitudes. The spatial structure of the warming rate in later decades resembles that obtained from straight line fitting over the whole temporal domain (see Fig. 2*h*). However, the later warming is much stronger than that determined by the straight line fitting method.

The zonally averaged trend (over only the land area) is plotted (Fig. 3) so that major features of the spatial–temporal evolution of the warming can be more evident. To eliminate the noisy pattern caused by spatially sporadic warming, we have applied a running mean over a 5º band in the meridional direction. The zonally averaged warming indeed had a three-band structure (Fig. 3). The noticeable zonally averaged warming (>0.2 K since 1900) first took place in the subtropical and subpolar regions of the Northern Hemisphere, followed by the subtropical warming in the Southern Hemisphere. In the Northern Hemisphere, this noticeable warming emerged in the northern subtropical and subpolar regions around 1920. The amplitude of the warming grew slowly for both bands, but the latitudinal scope of warming expanded toward midlatitude in the next three decades, and the 0.2 K lines of these two bands joined by around 1955. From 1955 onward, the warming accelerated at all latitudes. The greatest warming region in recent decades in the Northern Hemisphere was between the original high-latitude band and the subtropical band. However, these two bands can still be identified by the tongue-like extensions of the contours toward the left-hand side at about 26°N, 62°N, and 75°N.

In the Southern Hemisphere, the zonally averaged warming greater than 0.2 K in the subtropical band lagged that of the Northern Hemisphere and was relatively narrow in meridional width. It appears that the poleward warming expansion in the Southern Hemisphere is not as dominant as that of its Northern Hemispheric counterpart, a phenomenon that is possibly related to less land coverage in the Southern Hemisphere midlatitudes.

It is noted that the above evolution characteristics of the land surface air temperature trend of centennial and longer timescales cannot be revealed by analyzing only the later data (e.g., 1950 onward), for the multidecadal variability cannot be separated well from the trend of the later (shorter) data using any analysis method. There is also not enough evidence to argue that the extracted varying trend contains all the anthropogenic effect, for it has been demonstrated that multidecadal variability of land surface air temperature can be caused by natural or anthropogenic forcing of different timescales[16,22-26]. However, the slow-varying nature of the trend appears to be consistent with the slowly increasing carbon dioxide in the atmosphere.

Currently, we do not have explanations for why the global land surface trend has evolved as shown in Figs. 2 and 3. The relatively earlier warming in the subtropical regions suggests that the warming may be tied to changes in atmospheric circulations, which is consistent with the results of recent studies of the relation between global warming and changes in Hadley cells[27-29]. However, the greatest warming to date associated with (either linear or EEMD) trends occurs in the arid and semiarid regions of the midlatitude Northern Hemisphere, implying the small heat capacity of the arid and semi-arid regions may also have played a role[30]. The important physical reasons for why the warming trend evolves in this way remain to be investigated.

Corresponding Author: Dr. Zhaohua Wu, Department of Earth, Ocean and Atmospheric Science, Florida State University, Tallahassee, Florida 32306, USA. Email: zwu@fsu.edu

Acknowledgement: We thank reviewers for their constructive suggestions. This work was supported by the National Basic Research Program of China 2012CB955301 (FJ and JH) as well as the US National Science Foundation program AGS-1139479 (ZW and FJ).

Individual Contributions: All authors contributed to shaping up the ideas and writing the paper. The analyses were carried out by FJ and ZW, with various analysis methods designed by ZW. FJ and ZW are co-first authors.

Reference

1. IPCC *Climate Change 2007: The Physical Science Basis* (eds Solomon S. *et al.*) (Cambridge Univ. Press, 2007).
2. IPCC *Climate Change 2013: The Physical Science Basis* (http://www.ipcc.ch/, 2013).
3. Wu, Z., Huang, N. E. & Chen, X. The multi-dimensional ensemble empirical mode decomposition method. *Adv. Adapt. Data Anal*. **1,** 339–372 (2009).
4. Hansen, J., Ruedy, R., Sato, M. & Lo, K. Global surface temperature change. *Rev. Geophys.* **48,** RG4004 (2010).
5. Lawrimore, J. H. *et al.* An overview of the Global historical climatology network monthly mean temperature data set, version 3. *J. Geophys. Res.* **116,** D19121 (2011).
6. Wu, Z., Huang, N. E., Long, S. R. & Peng, C-K. On the trend, detrending and variability of nonlinear and non-stationary time series. *Proc. Nat. Acad. Sci. U.S.A.* **104,** 14889–14894 (2007).
7. Huang, N. E. *et al.* The empirical mode decomposition method and the Hilbert spectrum for non-stationary time series analysis. *Proc. R. Soc. Lond. A.* **454,** 903–995 (1998).
8. Huang, N. E. & Wu, Z. A review on Hilbert–Huang transform: the method and its applications on geophysical studies. *Rev. Geophys.* **46,** RG2006 (2008).
9. Wu, Z. & Huang, N. E. Ensemble empirical mode decomposition: a noise-assisted data analysis method. *Adv. Atmos. Sci.* **1,** 1–41 (2009).
10. Franzke, C. Multi-scale analysis of teleconnection indices: Climate noise and nonlinear trends analysis. *Nonlin. Processes Geophys.* **16,** 65–76 (2009).
11. Ruzmaikin, A. & Feynman, J. Search for climate trends in satellite data. *Adv. Adapt. Data Anal.* **1,** 667–679 (2009).
12. Qian, C., Wu, Z., Fu, C. B. & Zhou, T. J. On multi-timescale variability of temperature in China in modulated annual cycle reference frame. *Adv. Atmos. Sci.* **27,** 1169–1182 (2010).
13. Vecchio, A. & Carbone, V. Amplitude-frequency fluctuations of the seasonal cycle, temperature anomalies, and long-range persistence of climate records. *Phys. Rev. E.* **82,** 066101 (2010).
14. Franzke, C. & Woollings, T., On the persistence and predictability properties of North Atlantic climate variability. *J. Climate*. **24,** 466–472 (2011).

15. Fu, C., Qian, C. & Wu, Z. Projection of global mean surface air temperature changes in next 40 years: Uncertainties of climate models and an alternative approach. *Sci. China. Earth. Sci.* **54,** 1400–1406 (2011).
16. Wu, Z., Huang, N. E., Wallace, J. M., Smoliak, B. V. & Chen, X. On the time-varying trend in global-mean surface temperature. *Clim. Dynam.* **37,** 759–773 (2011).
17. Hu, Z. Z., Huang, B., Kinter III, J. L., Wu, Z. & Kumar, A. Connection of the stratospheric QBO with global atmospheric general circulation and tropical SST. Part II: Interdecadal variations. *Clim. Dynam.* **38,** 25–43 (2012).
18. Huang, B. *et al.* Influences of subtropical air-sea interaction on the multidecadal AMOC variability in the NCEP climate forecast system. *Clim. Dynam.* **39,** 631–555 (2012).
19. Zhu, J., Huang, B. & Wu, Z. The role of ocean dynamics in the interaction between the Atlantic meridional and equatorial modes. *J. Climate*. **25,** 3583–3598 (2012).
20. Misra, V., Li, H., Wu, Z. H. & DiNapoli, S. Global seasonal climate predictability in a two tiered forecast system: part I: boreal summer and fall seasons. *Clim. Dynam.* **42,** 1425–1448 (2014).
21. Mitchell, T. D. & Jones, P. D. An improved method of constructing a database of monthly climate observations and associated high-resolution grids. *Int. J. Climatol.* **25,** 693–712 (2005).
22. Semenov, V. A., Latif, M., Dommenget, D., Keenlyside, N. S., Strehz, A., Martin, T. & Park, W. The impact of North Atlantic-Arctic multidecadal variability on northern hemisphere surface air temperature. *J. Clim.* **23,** 5668–5677 (2010).
23. DelSole, T., Tippett, M. K. & Shukla, J. A significant component of unforced multidecadal variability in the recent acceleration of global warming. *J. Climate*. **24,** 909–926 (2011).
24. Booth, B. B., Dunstone, N. J., Halloran, P. R., Andrews, T. & Bellouin, N. Aerosols implicated as a prime driver of twentieth-century North Atlantic climate variability. *Nature* **484,** 228–232 (2012).
25. Tung, K. K. & Zhou, J. Using data to attribute episodes of warming and cooling in instrumental records. *Proc. Nat. Acad. Sci. U.S.A.* **110,** 2058–2063 (2013).
26. Zhang, R. *et al*. Have aerosols caused the observed Atlantic multidecadal variability? *J. Atmos. Sci*. **70,** 1135–1144 (2013).

27. Hudson, R. D., Andrade, M. F., Follette, M. B. & Frolov, A. D. The total ozone field separated into meteorological regimes–Part II: Northern Hemisphere mid-latitude total ozone trends. *Atmos. Chem. Phys.* **6,** 5183–5191 (2006).
28. Hu, Y. & Fu, Q. Observed poleward expansion of the Hadley circulation since 1979. *Atmos. Chem. Phys.* **7,** 5229–5236 (2007).
29. Seidel, D. J., Fu, Q., RanDel, W. J. & Reichler, T. J. Widening of the tropical belt in a changing climate. *Nature Geosci.* **1,** 21–24 (2008).
30. Huang, J., Guan, X. & Ji, F. Enhanced cold-season warming in semi-arid regions. *Atmos. Chem. Phys.* **12,** 5391–5398 (2012).

Figure Legends

Figure 1 | Spatial evolution of the EEMD trend of global land surface air temperature. Panels ***a*** to ***g*** represent EEMD trends ending at 1950, 1960, 1970, 1980, 1990, 2000 and 2009, respectively. Panel ***h*** displays the spatial structure of temperature increase based on time-unvarying linear trend over the whole data domain from 1901 to 2009. The underlying colorbar gives the temperature increase, with a unit Kelvin (K).

Figure 2 | Warming rate of global land surface air temperature. Panels ***a*** to ***g*** represent the instantaneous warming rate of the secular trend at 1950, 1960, 1970, 1980, 1990, 2000 and 2009, respectively. Panel ***h*** displays the spatial structure of the warming rate based on the time-unvarying linear trend over the whole data domain from 1901 to 2009. The underlying colorbar gives the warming rate, with a unit Kelvin per decade.

Figure 3 | Evolution of the zonally averaged trend of surface air temperature. The underlying colorbar gives the temperature increase, with a unit Kelvin (K). Note that color intervals are uneven.

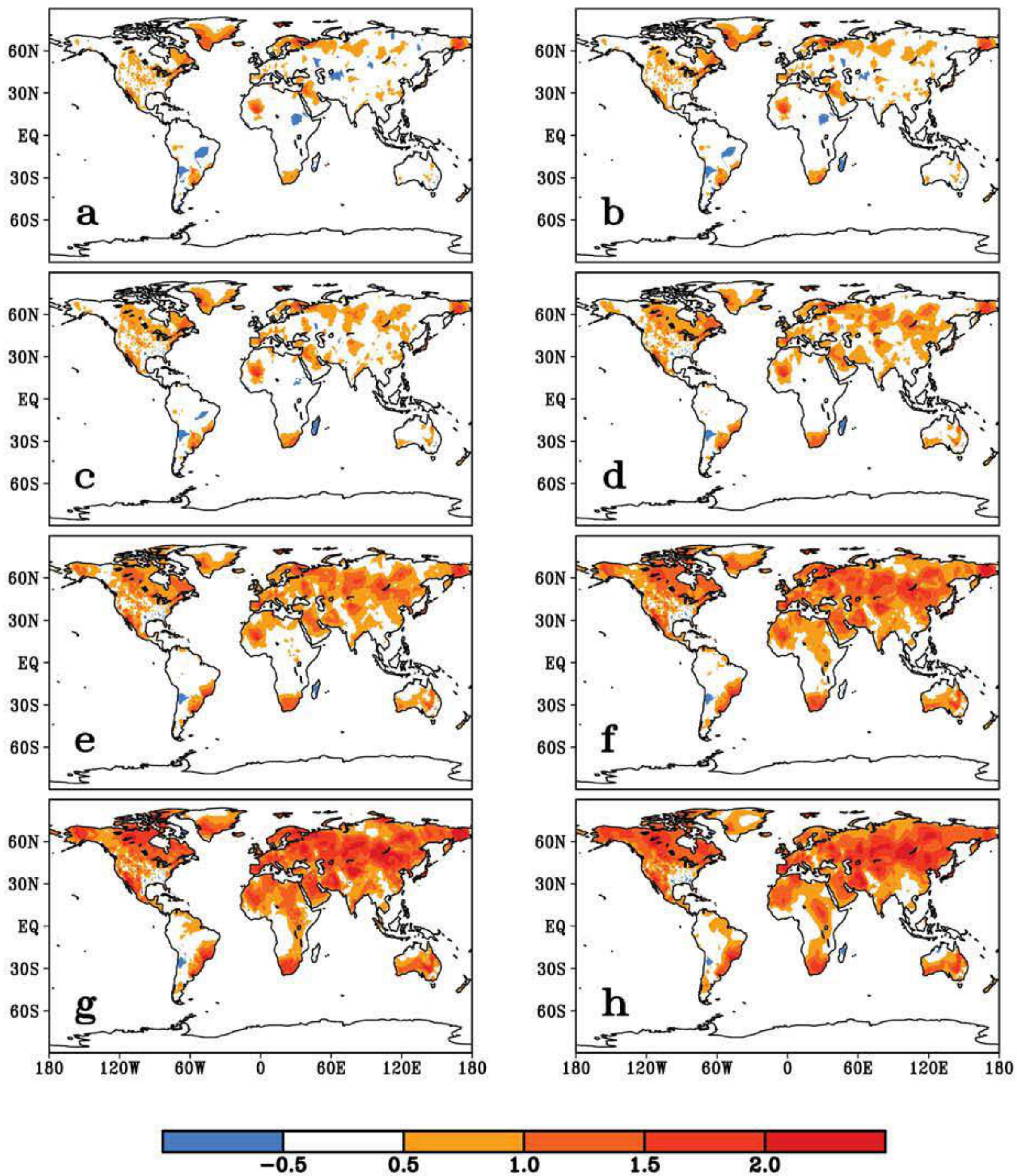
60N
30N
EQ
30S
60S
a
b
c
d
e
f
g
h
180
120W
60W
0
60E
120E
−0.5
0.5
1.0
1.5
2.0

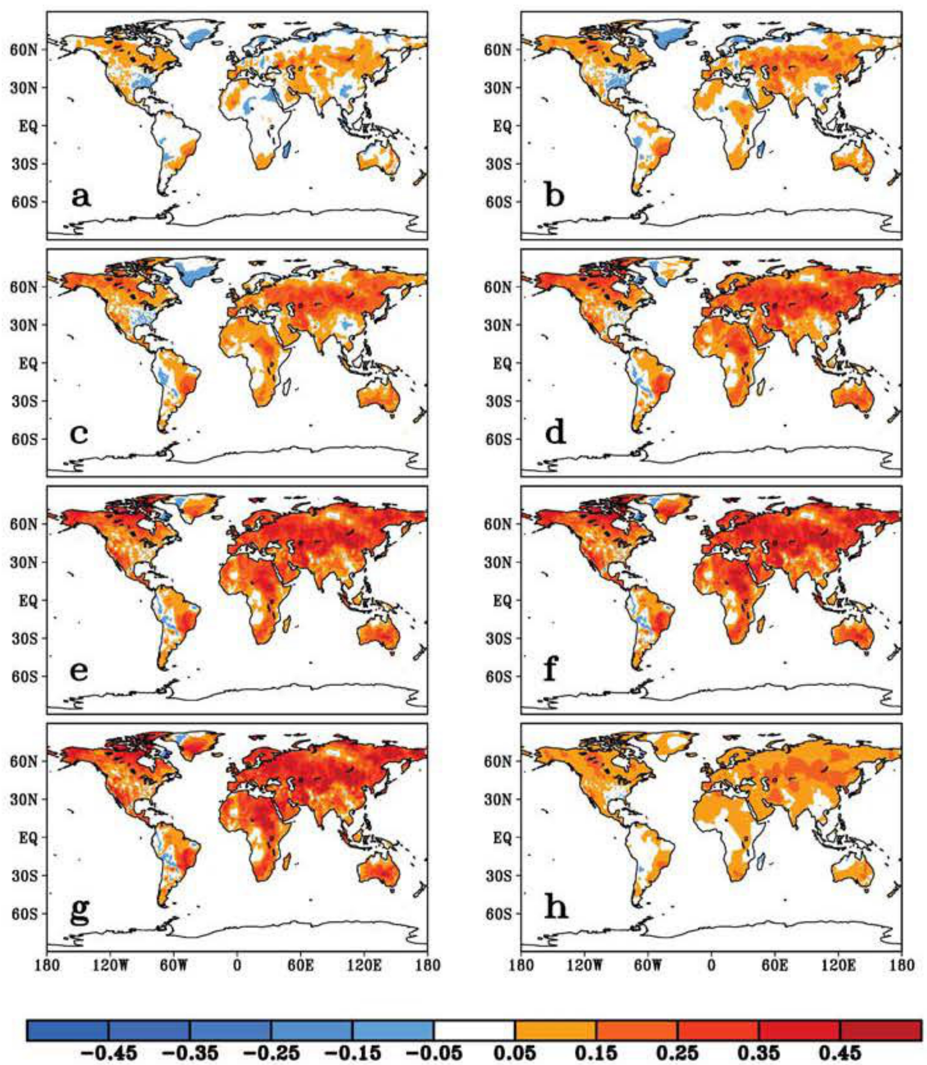

60N
30N
EQ
30S
60S
a
b
c
d
e
f
g
h
180
120W
60W
0
60E
120E
180
−0.45
−0.35
−0.25
−0.15
−0.05
0.05
0.15
0.25
0.35
0.45

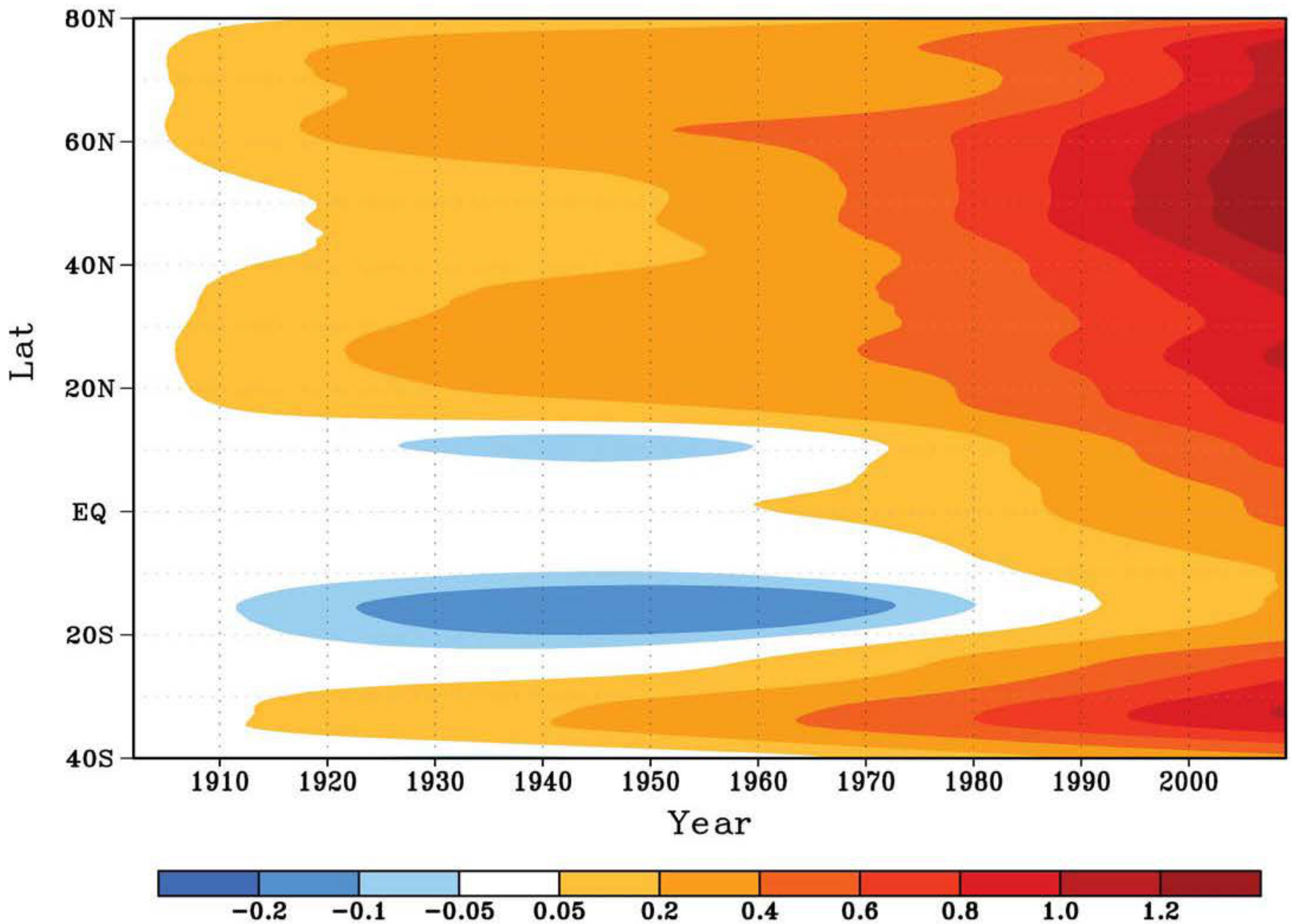
80N
60N
40N
20N
EQ
20S
40S
Lat
1910
1920
1930
1940
1950
1960
1970
1980
1990
2000
Year
−0.2
−0.1
−0.05
0.05
0.2
0.4
0.6
0.8
1.0
1.2